Ensemble average method for runtime saving in Large Eddy Simulation of free and Ducted Fuel Injection (DFI) sprays

Fuel 344 (2023) 128110

Contents lists available at ScienceDirect

Fuel

journal homepage: www.elsevier.com/locate/fuel

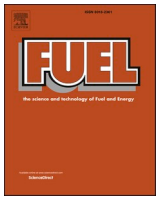

Full Length Article

Ensemble average method for runtime saving in Large Eddy Simulation of free and Ducted Fuel Injection (DFI) sprays

C. Segatori [a], A. Piano [a,*], B. Peiretti Paradisi [a], F. Millo [a], A. Bianco [b]

[a] Politecnico di Torino, Energy Department, Italy
[b] Powertech Engineering S.r.l., Italy

ARTICLE INFO

Keywords:
Computational Fluid Dynamics
Large Eddy Simulation (LES)
Turbulence modelling
Spray
Ducted Fuel Injection

ABSTRACT

Computational Fluid Dynamics (CFD) with Large Eddy Simulation (LES) turbulence model is a valuable tool to investigate complex problems. However, for high Reynolds number problems, the associated huge computational cost often leads researchers to the use of more simplified and less accurate approaches, especially if statistics is needed for the generalization of the results and comparison against experimental data. Therefore, the introduction of innovative methodologies to reduce the computational cost maintaining results reliability would be of paramount importance for LES-based investigation.

In this context, the aim of this work is to assess a runtime saving methodology to ensemble average several axial symmetric spray simulations obtained with LES. In particular, the number of independent samples for the average procedure has been increased by exploiting the axial symmetry characteristics of a diesel spray case study, extracting more realizations from a single simulation. This ensemble average approach was compared with the standard one, based on one realization per simulation, at equal statistical sample size. Main spray physical quantities and turbulence characteristics were examined, both globally and locally. The same procedure was also applied to a different diesel-relevant spray configuration, known as ducted fuel injection.

The reliability of this ensemble average methodology has been herein proven for both spray configurations, highlighting a dramatic runtime saving without any worsening of the accuracy level. In particular, this approach, as applied in this work, guaranteed a computational cost reduction of 50–75%. Thereby, the present methodological assessment could motivate researchers involved in the investigation of spray processes to undertake the path of statistically significant LES analysis.

1. Introduction

Many applications in technical and industrial fields are based on spray processes for improving mixing, cooling, and other phenomena. Considering the injection of a liquid-phase fluid into a gas-phase fluid, the spray is a dynamic collection of drops dispersed in a gas, whose size varies according to the application, undertaking several complex phenomena, like cavitation, drop breakup, drop drag, collision and coalescence, evaporation, turbulent dispersion, and so on. Given this complexity, spray comprehensive and thorough understanding is typically difficult, together with the subsequent optimization for each application, thus urging the usage of Computational Fluid Dynamics (CFD) tools for this purpose. In particular, enabling virtual access to any process or state variable at any location and time instant, CFD simulations integrated with spray models, properly validated against experimental data, represent a powerful tool providing insight into spray complex processes [1].

In the context of diesel engines, the optimization of the fuel spray exiting the injector nozzle is of paramount importance to ensure a high quality of the fuel/air mixture in the combustion chamber, affecting

Abbreviations: AMR, Adaptive Mesh Refinement; aSOI, after Start of Injection; CFD, Computational Fluid Dynamics; CFL, Courant-Friedrichs-Lewy; CVV, Constant-Volume Vessel; DFI, Ducted Fuel Injection; DNS, Direct Numerical Simulation; LES, Large Eddy Simulation; LES-NWM, Large Eddy Simulation with Near Wall Modelling; LOL, Lift-Off Length; LSR, Length Scale Resolution; MSI, Magnitude Similarity Index; RANS, Reynolds-Averaged Navier-Stokes; RMS, Root Mean Square; SGS, Sub-Grid Scale; SMD, Sauter Mean Diameter; SSI, Structure Similarity Index; TKE, Turbulent Kinetic Energy; TRI, Turbulence Resolution Index; |V|, Velocity magnitude; η, Kolmogorov length scale; ϕ, Equivalence ratio; < >, Ensemble average.

* Corresponding author.
E-mail address: andrea.piano@polito.it (A. Piano).

https://doi.org/10.1016/j.fuel.2023.128110
Received 12 December 2022; Received in revised form 7 March 2023; Accepted 8 March 2023
Available online 28 March 2023

both the combustion and the pollutant formation processes [2]. In particular, the target is to improve the mixture preparation upstream of the auto-ignition zone, whose local characteristics drastically affect the combustion outcome and determine the soot formation in the diesel flame [3,4]. For this purpose, several experiments and CFD simulations are usually performed in test vessels (i.e., instead of the engine combustion chamber), equipped with a single-hole coaxial injector, to investigate the diesel spray behaviour at a more fundamental level [5].

Focusing on the injection conditions typical of a diesel spray, the turbulence plays an important role, whose description should be thus accurate in the CFD simulations. The widely used approach for turbulence modelling is the Reynolds-Average Navier Stokes (RANS) one, consisting in time-averaging the Navier-Stokes (NS) equations. This simplified approach is computationally effective but prevents a fine description of the physical mechanisms due to its inherent averaging nature [6]. Furthermore, by adopting the RANS approach, the turbulence is modelled for the entire spectrum of turbulent structures. Therefore, the reliability of the employed model for each case study is crucial to obtain physical and accurate results. However, the values of the models parameters are far from universal [1,7]. These aspects make this approach weaker for studies of a fundamental character, like the spray processes understanding and improvement. For this purpose, when computational and time resources are sufficient, the Large Eddy Simulation (LES) approach is typically the best option. With LES, the effect of the largest scales (which are primarily affected by boundary conditions) is directly computed from the NS equations, while only the small sub-grid scales are modelled. Since small scales tend to be more isotropic than the largest ones, the related employed models are simpler and more universal than the typical RANS models [8,9].

However, the computational cost associated with a single LES is higher than an equivalent RANS because of several reasons, among them the need for a finer grid in order to resolve the whole energy-containing range of the turbulent spectrum, and thus to avoid falling in the Very Large Eddy Simulation (VLES) field, losing accuracy [10]. This computational cost is even increased by the need for statistics when LES is employed. Indeed, each LES can be classified as a numerical experiment, highly affected by a small variation of initial conditions or random processes, thus leading to run-to-run variability, as well as in experimental campaigns. Therefore, a sufficient number of realizations (N) is needed to properly compute the ensemble average, for general quantification and comparison purposes, thus raising the computational cost by N-times and making the LES approach often prohibitive, especially for industrial analysis.

In light of this, runtime saving methodologies for statistical LES analysis can be of paramount importance for the CFD investigation of diesel sprays. Considering the abovementioned test vessel case study, the axial symmetry characteristics of the domain could be exploited to reduce the number of simulations needed to reach the targeted number of samples, adopting an averaging method as proposed in the literature by [11,12]. The basic idea is to consider, for each simulation, a certain number of semi-slices (M) parallel to the spray axis and assume that each semi-slice behaves as a different numerical experiment. In this way, the computational cost would be potentially reduced by M−times. This concept is quite similar to the spatial average, already employed in the literature about axial symmetric sprays to determine important spray/flame quantities [13,14]. However, a thorough demonstration of this averaging concept is not present in the literature according to the Authors' knowledge.

Therefore, the aim of this work is to assess the abovementioned runtime saving methodology to ensemble average several axial symmetric spray simulations obtained with LES. In particular, the performance of the presented approach is evaluated in terms of accuracy of the main spray physical quantities and turbulent characteristics, and the main limitations and best practices to avoid unwanted fictitious impacts on the results are discussed. For this purpose, the methodology is validated against the conventional ensemble average approach, at an equal number of samples for the average, considering a non-reacting diesel spray test vessel case study available in the scientific literature [15,16]. An application of the same procedure is also reported for a different diesel-relevant spray concept, termed Ducted Fuel Injection (DFI), nowadays under study to suppress soot emissions in diesel combustion [17]. In this configuration, a small duct is assembled co-axially at a certain distance downstream of the injector nozzle, satisfying the axial symmetry hypothesis for the application of the method. This latter case study was employed to verify if the interaction between spray and duct wall could affect the capability of the proposed ensemble average method to provide accurate results.

2. Methodology

2.1. Case study

The case study considered for the assessment of the above-described ensemble average method is a diesel spray in Constant-Volume Vessel (CVV) under the non-reacting operating conditions summarized in Table 1. The injector hole is a prototype single-hole Common Rail injector for compression-ignition engine applications, featuring a nozzle diameter equal to 0.180 mm.

This case is detailed in [15,16], where a free spray configuration was compared with the DFI concept in CVV. For the present work, both configurations are studied, starting with the former more general one. A total simulation duration of 1 ms is considered, including 0.7 ms of the injection event. The simulation duration is sufficient to obtain the whole visualization of the spray evolution along the length of the optical access window, featuring the experimental campaign in [15,16].

2.2. 3D-CFD simulation setup

The 3D-CFD work was carried out by means of the commercially available software CONVERGE CFD V3.0.14 [18]. Compared to previous studies, the cylindrical CVV has been downsized to curtail unnecessary computational costs, carefully verifying the absence of impact on the solution.

The spray model was the same developed in the RANS framework [15,16,19], extensively validated against experimental data in both free spray and DFI configuration. The main characteristics and sub-models are reported in Table 2.

As explained in [15], the calibration process was mainly focused on the time and size constants of the modified KH-RT breakup model (i.e., without the breakup length) and on the discharge coefficient, which was properly modified taking into consideration the super-cavitation hypothesis deeply investigated in [25] for similar injector configurations.

For the turbulence modelling, the LES approach was employed, allowing to directly resolve the largest turbulent scales, while the Sub-Grid Scale (SGS) remains modelled. In this case, the one-equation dynamic structure model was used for the SGS, a non-viscosity model offering the advantage of not requiring *a priori* knowledge of the flow coefficients, which are dynamically determined as a function of time and space from the resolved field [26,27]. In particular, it directly estimates the stress tensor of the NS momentum equation, instead of modelling the viscosity term, and adds a transport equation for the SGS kinetic energy to provide scaling and enforce a budget on the energy flow between the resolved and the sub-grid scales [28]. In this way, the model can reliably

Table 1
Operating conditions.

Vessel pressure	20 bar
Vessel temperature	773 K
Rail pressure	1200 bar
Injection duration	1.5 ms
Injected mass	11.85 mg

Table 2
3D-CFD Spray model summary.

Injected fuel	Diesel #2
Evaporating species	N-Heptane (N-C7H16)
Liquid injection	Blob model [20]
Droplet turbulent dispersion	O'Rourke model [21]
Spray breakup	Modified KH-RT model [22]
Evaporation	Frossling with boiling model [21]
Droplet drag	Dynamic drop drag model [23]
Heat transfer	O'Rourke and Amsden model [24]

estimate the SGS Turbulent Kinetic Energy (TKE), which is of interest for a quantitative evaluation of the grid quality. The grid size is critical, since acts as a spatial filter (i.e., low pass filter in the frequency domain), defining the smallest resolved turbulent scales and, thus, the quality of the LES resolution. The results are gradually less affected by the SGS modelled part as the filter is shifted towards smaller structures, guaranteeing that the best solution is approached as the grid size is reduced.

The computational domain was entirely meshed with a cartesian grid by means of the CONVERGE CFD patented cut-cell technique. This approach has several advantages such as the relatively low simulation setup time, the easiness to automate, and the possibility to execute consistent grid sensitivity analysis, essential for LES mesh setup, with accuracy and computational cost directly related [29]. A base grid of 2 mm was defined, gradually refined towards the spray region through fixed refinement regions: a first cylinder of 250 μm grid size covering the extension of the experimental optical access window [15], and a second cylinder of 125 μm grid size for the first 30 mm of penetration (i.e., *near-spray region*). Furthermore, the Adaptive Mesh Refinement (AMR) tool was enabled, achieving a minimum grid size of 62.5 μm in the most critical areas, whose detection is based on velocity gradients. These grid settings are graphically illustrated in Fig. 1.

In order to ensure a good LES solution, a minimum grid size capable to resolve at least 80% of the turbulent structures in the whole domain was targeted, as indicated by [10,30]. The 62.5 μm minimum grid size definition resulted from a grid sensitivity analysis, performed by sweeping the minimum grid size from 125 μm to 31.25 μm, keeping constant the base grid while modifying the embedding refinement level accordingly to maintain the same scale factors, as reported in Table 3.

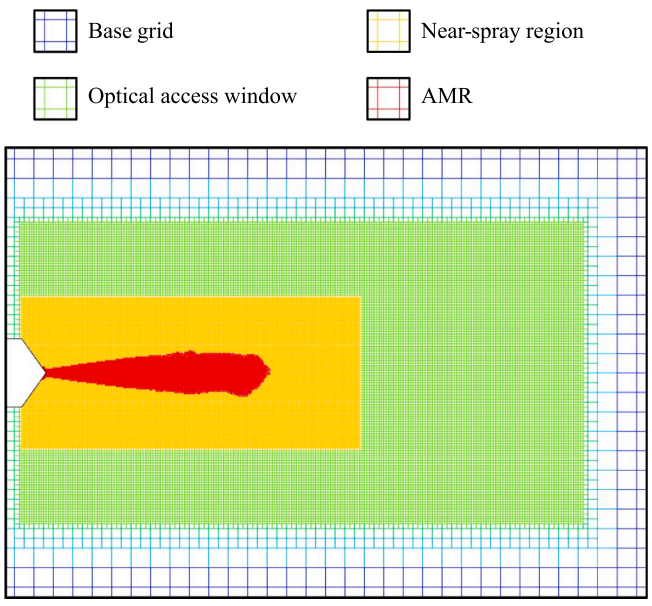

Fig. 1. Grid discretization and refinements employed for the numerical activity. The base grid, the fixed refinement regions and the AMR outcome are illustrated at 0.1 ms aSOI. Minimum grid size: 62.5 μm.

Table 3
Grid settings employed for the sensitivity analysis to the grid size. Minimum grid size swept from 125 μm to 31.25 μm.

Minimum grid size	Base grid	Optical access window	Near-spray region	AMR
125 μm	2 mm	500 μm	250 μm	125 μm
62.5 μm	2 mm	250 μm	125 μm	62.5 μm
31.25 μm	2 mm	125 μm	62.5 μm	31.25 μm

As indicated by [31], the number of injected parcels was increased as the mesh was refined to avoid an overestimation of the liquid penetration due to an excessive amount of parcel mass in a single cell. In particular, 2 million parcels were injected for the 125 μm case, 8 million for the 62.5 μm case, and 21 million for the 31.25 μm case. This increment in the number of parcels contributed to the increase of the computational cost as the grid was refined, together with the higher number of cells and the lower minimum time step. In Fig. 2, maximum number of computational cells, minimum resolution time-steps, and requested core hours for a single realization are reported as a function of the minimum grid size. The core hours values are based on the utilization of Intel Xeon Scalable Processors Gold 6130 2.10 GHz.

The reduction of the grid size from 125 μm to 31.25 μm led to an increment of the number of computational cells (Fig. 2(a)) of slightly less than two orders of magnitude, while the variable time-step (Fig. 2 (b)), dynamically determined by the Courant-Friedrichs-Lewy (CFL) limits, was reduced of about an order of magnitude. These factors resulted in a dramatic raise of the core hours requested by the computation: more than two orders of magnitude passing from 125 μm to 31.25 μm (Fig. 2(c)). It is worth noting that, due to the high number of realizations needed for statistical convergence, the finest grid would require a prohibitive number of core hours in absolute values.

In Fig. 3, the velocity magnitude and equivalence ratio (ϕ) fields of a single realization at 0.3 ms after Start of Injection (aSOI) are depicted on a plane passing for the spray axis for each considered grid size. The ϕ is defined as the ratio of the current fuel-to-air ratio over the fuel-to-air ratio required for complete stoichiometric combustion. The injector nozzle is located at r = 0 mm, Z = 0 mm.

Focusing on the velocity magnitude field (Fig. 3 – left), it can be observed that reducing the grid size (from the top to the bottom) means a more detailed description of the small vortices, particularly evident towards the spray tip. The higher number of small vortices resolved tends to affect the spray breakup and mixing process which have an impact on the spray penetration. Indeed, moving from the 125 μm grid to the 62.5 μm grid, the penetration is slightly lower. A further refinement seems not necessary in terms of penetration, in fact, the spray tip location for the 31.25 μm grid is similar to the 62.5 μm grid. However, the core of the jet features different values also among the latter two grids. Indeed, the high-speed core depicted in red colors is less extended for the 31.25 μm grid, compared to the 62.5 μm one. This is due to the fact that the jet core is the part that interacts less effectively with the surrounding environment, and thus tends to be more compact unless the effect of the smallest length scales is well-described. Furthermore, the reduction of the grid size has also an effect on the injection velocity, which in turn can affect the jet core breakup behaviour. In fact, the smaller the grid size, the higher the number of interfacial cells contained in the injector nozzle area and, thus, the larger the amount of liquid volume fraction at the nozzle exit. A liquid volume fraction equal to 1 at the nozzle exit is desirable to correctly capture the injection velocity, if able to guarantee the numerical stability of the simulation. Since the current methodology utilizes a fully implicit liquid–gas momentum coupling approach to keep the simulations stable in the presence of high liquid volume fractions, the finer the grid size, the more accurate the injection velocity. To better visualize this effect, a close-to-injector zoom of the velocity magnitude (|V|) axial values as function of the axial

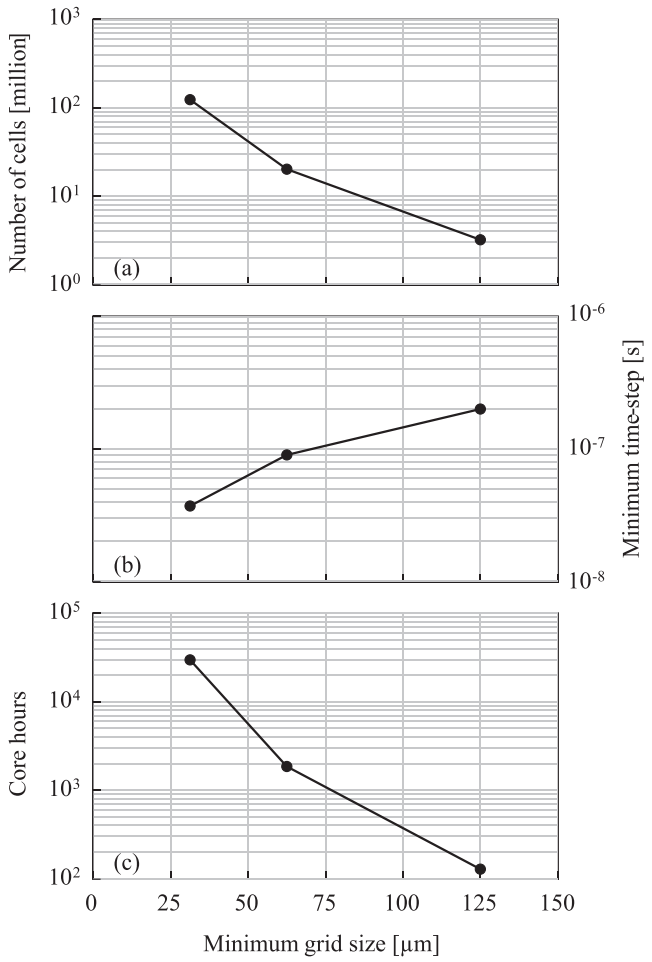

Fig. 2. Sensitivity analysis to the grid size: (a) maximum number of computational cells, (b) minimum resolution time-steps, and (c) requested core hours for a single realization as a function of the minimum grid size. Processors: Intel Xeon Scalable Processors Gold 6130 2.10 GHz.

distance is reported in Fig. 4 for the three considered grid configurations at 0.3 ms aSOI.

Observing the first 3 mm, the distance between the nozzle and the highest velocity values tends to be gradually shorter as the grid is refined. Nevertheless, no remarkable improvement can be detected moving from the 62.5 μm grid (solid line) to the 31.25 μm grid (dotted line), meaning that this effect could be sufficiently well-described by the intermediate grid.

Moving to the ϕ distribution (Fig. 3 – right), from an overall perspective the intermediate grid size (62.5 μm) is close to the convergence, showing similar penetration and shape of the spray tip to the most refined grid (31.25 μm), while the coarsest one (125 μm) features a more stretched shape, overestimating the spray tip penetration. However, considering the rich core, similar considerations to the velocity magnitude distribution can be given. For the 125 μm grid, the jet core does not show vortex structures up to Z = -40 mm, thus remaining more compact and characterized by high ϕ values up to Z = -50 mm. Some vortices are involved in the jet core when an intermediate grid size of 62.5 μm is considered, reducing this length of breakup to about 45 mm. Nevertheless, the most refined grid (31.25 μm) leads to a more detailed turbulent description of the rich jet core.

According to these results, the 125 μm grid must be discarded for inaccuracy reasons, while the 62.5 μm grid emerged as a possible option, able to well predict the overall spray behaviour at a reasonable computational cost, forgoing an accurate quantification of certain local values, like the equivalence ratio in the core of the jet, for which 31.25 μm turbulent length scale resolution seems needed. Nevertheless, in order to make this choice methodologically robust, a more quantitative assessment was carried out. According to Piscaglia et al. [32], a reasonable turbulence resolution is achieved when the Length Scale Resolution (LSR) parameter, defined as the ratio between the resolved energy level and the corresponding lower limit of the inertial subrange, respects the limit in equation (1):

$$LSR = \frac{\Delta}{60\eta} < 3 \div 5 \tag{1}$$

where Δ is the filter size, here coincident with the minimum grid size, while η is the Kolmogorov length scale which can be estimated as in equation (2) [10]:

$$\eta \simeq \frac{L_0}{Re^{\frac{3}{4}}} \tag{2}$$

where L_0 is the characteristic dimension of the phenomenon and Re is the Reynolds number. Considering the conditions encountered by the spray at 10 mm from the injector nozzle, the characteristic dimension can be assumed equal to the corresponding spray diameter (approx. 2.7 mm). By assuming the average values of kinematic viscosity (approx. 2.7 · 10^{-6} m^2/s) and velocity (approx. 150 m/s) on the spray cross-section, the Reynold number results equal to 1.25 · 10^5, leading to an estimated Kolmogorov length scale of approximately 0.41 μm. Therefore, considering the 62.5 μm grid size, the LSR parameter results to be equal to 2.5, thus respecting the upper limit of equation (1).

Finally, a further *a posteriori* evaluation is possible by exploiting the SGS TKE in output from the dynamic structure SGS model. As above-mentioned, a lower limit of turbulent structures resolution, equal to 80% in the whole domain, is suggested in [10,30] to obtain accurate LES results. This can be evaluated by defining a local index, herein termed Turbulence Resolution Index (TRI), as the ratio between the resolved TKE and the total TKE (i.e., resolved plus sub-grid scale TKE), as in equation (3):

$$TRI = \frac{TKE_{resolved}}{TKE_{resolved} + TKE_{SGS}} > 0.8 \tag{3}$$

TRI is equal to 0 for a RANS simulation, where all the turbulence is modelled, while is equal to 1 for a Direct Numerical Simulation (DNS), where all the turbulence is resolved by definition. As explained in [10], the resolved TKE was calculated starting from the Root Mean Square (*RMS*) of the velocity fluctuations components (equations (4) and (5)), hence an ensemble average among a sufficient number of samples must be performed for this evaluation.

$$TKE_{resolved} = \frac{1}{2}\left(RMS_u^2 + RMS_v^2 + RMS_w^2\right) \tag{4}$$

$$RMS_{u,v,w} = \sqrt{< (u', v', w')^2 >} \tag{5}$$

Each velocity fluctuation component (u', v' and w') is computed as the difference between the velocity value (u, v and w) of sample i and the ensemble-averaged value ($<u>$, $<v>$ and $<w>$) considering all the available samples, as in equation (6):

$$(u', v', w')_i = (u, v, w)_i - (<u>, <v>, <w>) \tag{6}$$

In Fig. 5, the TRI for the 62.5 μm grid size at 0.7 ms aSOI (pseudo-stationary conditions) is depicted on a plane passing for the spray axis. 20 realizations are herein considered for the ensemble average and the corresponding resolved TKE calculation. The periphery of the spray plume is highlighted with a red band, defined by all the ϕ values falling between 0.1 and 0.2.

It can be observed that the entire spray region (i.e., within the red ϕ band in Fig. 5) is characterized by a TRI remarkably higher than the 0.8 limit, demonstrating a good LES resolution with the chosen grid size in the whole domain of interest. The grey color, showing computational

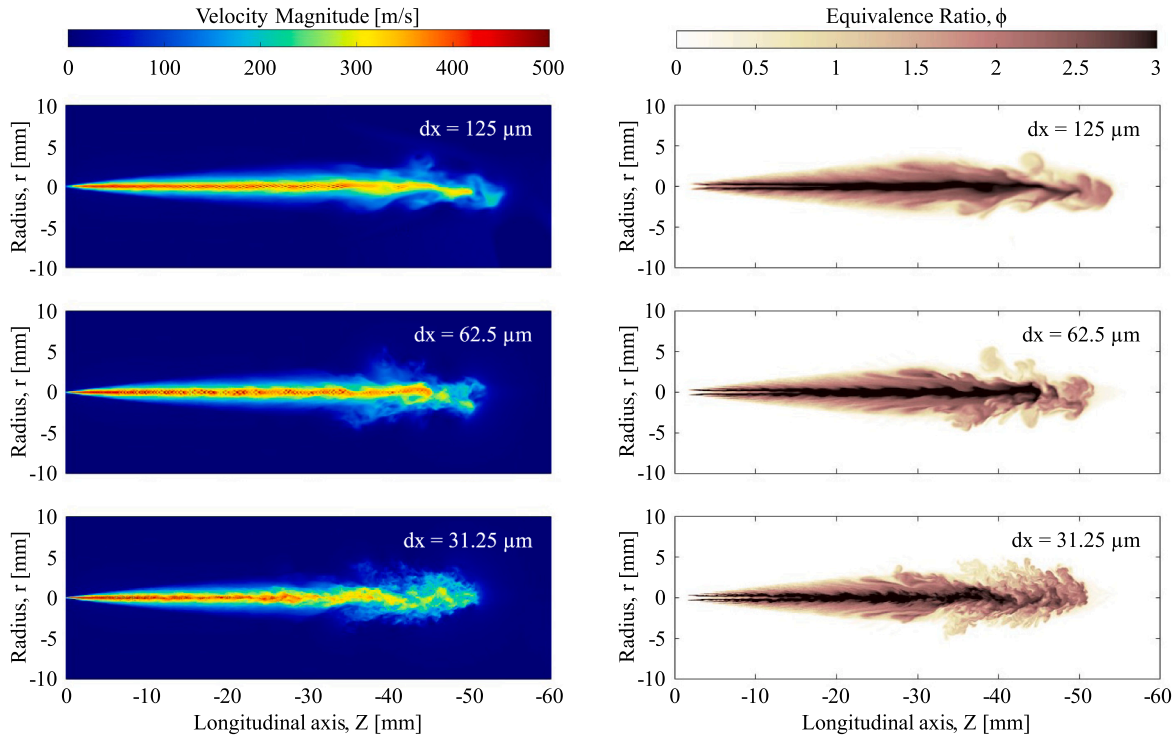

Fig. 3. Sensitivity analysis to the grid size: Velocity magnitude (left) and equivalence ratio (right) distributions of a single realization on a section passing for the spray axis at 0.3 ms aSOI as a function of the minimum grid size.

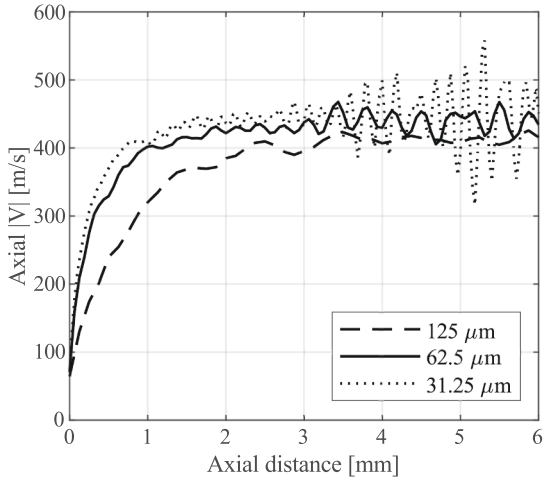

Fig. 4. Velocity magnitude axial values of a single realization as a function of the axial distance at 0.3 ms aSOI for three different grid sizes: 125 µm (dashed line); 62.5 µm (solid line); 31.25 µm (dotted line).

cells below the above-defined threshold, is always referred to locations in which a very low turbulence level is expected.

In conclusion, the 62.5 µm grid size was considered suitable for the purpose of the work, being able to sufficiently resolve the turbulent eddies from both a qualitative and a quantitative point of view, limiting the computational cost to a reasonable level.

2.3. Ensemble average approaches

The aim of this work is to assess a runtime saving methodology to ensemble average several axial symmetric spray LES simulations. Considering a cylindrical test vessel equipped by a single-hole injector coaxial to the cylinder axis, the conventional approach (herein named *Standard approach*) consists in deriving a certain number of statistical samples (N) by running S = N simulations, varying either initial conditions or random seed parameters. Nevertheless, considering a certain number (M) of semi-slices containing the spray axis, and assuming that each semi-slice behaves as a different numerical experiment, if statistical independence is ensured by a sufficient angular distance among semi-slices, the same number of statistical samples (N) can be achieved by S = N/M simulations. This approach (herein named *Multi-Slice approach*) would enable a drastic reduction of computational costs, with the drawback of limiting to a 2D representation of the results, which is however generally used for axial symmetric problems. For the sake of clarity, a schematic representing the two considered ensemble average methods is reported in Fig. 6, considering M = 4 for the multi-slice approach.

It is important to note that an underlying hypothesis, to be verified along this work, is that the effect on turbulent fluctuations induced by a different initialization is comparable with the one induced by a different angular position.

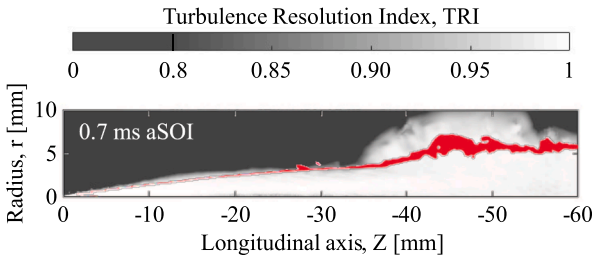

Fig. 5. Turbulence Resolution Index (TRI) distribution on a section passing for the spray axis at 0.7 ms aSOI for the 62.5 µm grid size, considering an ensemble average among 20 statistical samples. The area with an equivalence ratio value between 0.1 and 0.2 is overlapped in red. (For interpretation of the references to color in this figure legend, the reader is referred to the web version of this article.)

In order to consistently compare the standard approach and the multi-slice approach, introduced above, the same number of realizations has been considered. In this context, a single realization is represented by a statistically independent semi-slice, passing through and tangential to the symmetry axis. In Table 4, the details related to the considered number of simulations, number of realizations, and resulting computational costs are reported. The computational cost is based on the utilization of Intel Xeon Scalable Processors Gold 6130 2.10 GHz.

A target number of 20 realizations was considered for both approaches. For the standard approach, it was obtained through 20 different simulations, leading to a total runtime of approximately 1520 core days on the available High-Power Computing resources. For the multi-slice approach, the chosen number of semi-slices per simulation deals with two main aspects. On one hand, statistical independency among samples must be ensured by a sufficient angular distance among semi-slices: according to Farrace et al. [11], a number of semi-slices lower than 10–12 enables sufficiently low spatial autocorrelation values for the azimuthal velocity, apart from the region close to the axis. On the other hand, the use of a cartesian grid for the resolution of the flow field can induce some numerical asymmetries, thus not caused by the physics of the problems. Hence, even though these grid-induced asymmetries are typically not taken into account for similar problems in literature, only orthogonal semi-slices, aligned with the resolution grid, were herein considered to make this methodological assessment as robust as possible in its conclusions. Indeed, although the variations induced on the main physical quantities (e.g., absolute velocity values, pressure, etc.) can be considered neglectable, very slight non-physical deviations can instead largely affect the resolved TKE computation, being based on the RMS of the velocity fluctuations. Therefore, a conservative value of 4 orthogonal semi-slices was considered for each simulation, making 5 simulations necessary to reach the target number of realizations, with an associated 75% potential runtime reduction.

The final value of 20 realizations for each approach was chosen after a statistical convergence analysis adopting the standard ensemble average approach. In particular, the ensemble average variability distribution ($\Delta < (r,Z) >$) as a function of the considered number of samples (i) was evaluated for both the velocity magnitude ($|V|$) and the equivalence ratio (ϕ), as in equations (7) and (8).

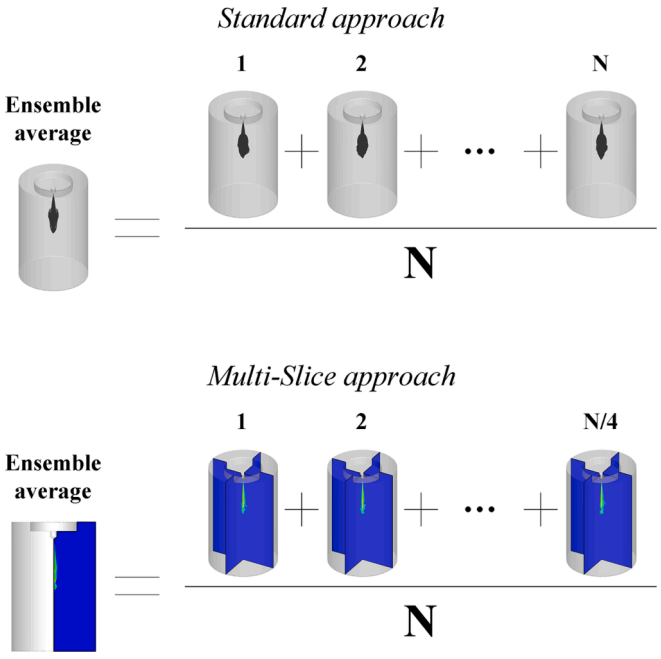

Fig. 6. Sketch of the ensemble average method through both the standard approach (top) and the multi-slice approach (bottom), considering 4 samples per simulation (M = 4 semi-slices).

$$\Delta < |V|(r,Z)>_{i+1} = < |V|(r,Z)>_{i+1} - < |V|(r,Z)>_{i} \quad (7)$$

$$\Delta < \phi(r,Z)>_{i+1} = < \phi(r,Z)>_{i+1} - < \phi(r,Z)>_{i} \quad (8)$$

In other words, the local variations between the ensemble average of *i+1* samples and the ensemble average of *i* samples were computed for both ϕ and $|V|$ up to $i+1 = 20$, and the outcome for the ϕ field on five steps (i.e., every four samples) is reported in Fig. 7, together with the frequency distribution in logarithmic scale.

The regions of the spray with a $\Delta<\phi>$ higher than 0.1 with respect to the previous averaging step are highlighted with a saturated grey color, while the regions which tend to stabilize to a final value (i.e., negligible variation considering a further sample for the average) are gradually whiter as the number of samples increases. The higher the number of samples, the whiter the whole spray picture. In particular, focusing on the first part of the spray (i.e, less than 30 mm distance from the nozzle), about 8–12 samples could be deemed sufficient to obtain stabilization of the average. Nevertheless, moving to the highly turbulent region (i.e., more than 30 mm distance from the nozzle), higher variability is present, and the saturated grey locations seem attenuated only after more than 16 samples, thus motivating the usage of 20 samples. This conclusion can be drawn also from the frequency distribution histograms (right): it is quite evident how the distribution becomes gradually more compact as the number of samples increases, moving towards 100% the bin related to the lowest error, and zeroing the bin $|<\phi>| > 0.1$ only when 20 samples are considered.

To obtain a more quantitative and aggregate visualization of this variability for both ϕ and $|V|$, in Fig. 8, the average and the maximum values of the variability distributions as a function of the number of considered realizations are reported for a transient (0.3 ms aSOI) and a pseudo-stationary (0.7 ms aSOI) time instants. In this computation, only the computational cells belonging to the spray structure (based on a ϕ criterion) for the i and $i+1$ samples averages are taken into account. A logarithmic scale is employed for the data visualization.

Focusing on the $|\Delta<|V|>|$ trends (Fig. 8, top), both the maximum and the average variability values are decreased by about an order of magnitude passing from 2 to 20 samples for the averaging process. In particular, the variability decreases almost linearly on the logarithmic scale at the beginning, while tends to plateau approaching 20 samples, suggesting that a much larger number of samples would be needed to obtain the variability reduction of another order of magnitude. This behaviour is similar during both the transient and the pseudo-stationary phases. Moving to the $|\Delta<\phi>|$ trends (Fig. 8, bottom), similar conclusions can be drawn confirming the final choice of 20 realizations asstatistical sample size.

Since, from a theoretical point of view, an infinite number of samples is needed to achieve statistical convergence (i.e., perfectly stable ensemble average), stability thresholds on both the average and the maximum values are herein evaluated to well-define the accuracy limits under which the adopted average on 20 samples is valid. These thresholds (red horizontal lines in Fig. 8) were defined, considering each time instant, as the approximated upper limit for the variability of the ensemble average on 20 samples, capable of simultaneously including the previous four steps, for continuity and stability reasons. In the end,

Table 4
Number of simulations, number of realizations, and total runtime considered for the standard and the multi-slice ensemble average approaches. Processors: Intel Xeon Scalable Processors Gold 6130 2.10 GHz.

Ensemble average approach	Simulations	Semi-slices / simulation	Realizations	Total runtime
Standard	20	1	20	≈1520 core days
Multi-Slice	5	4	20	≈380 core days

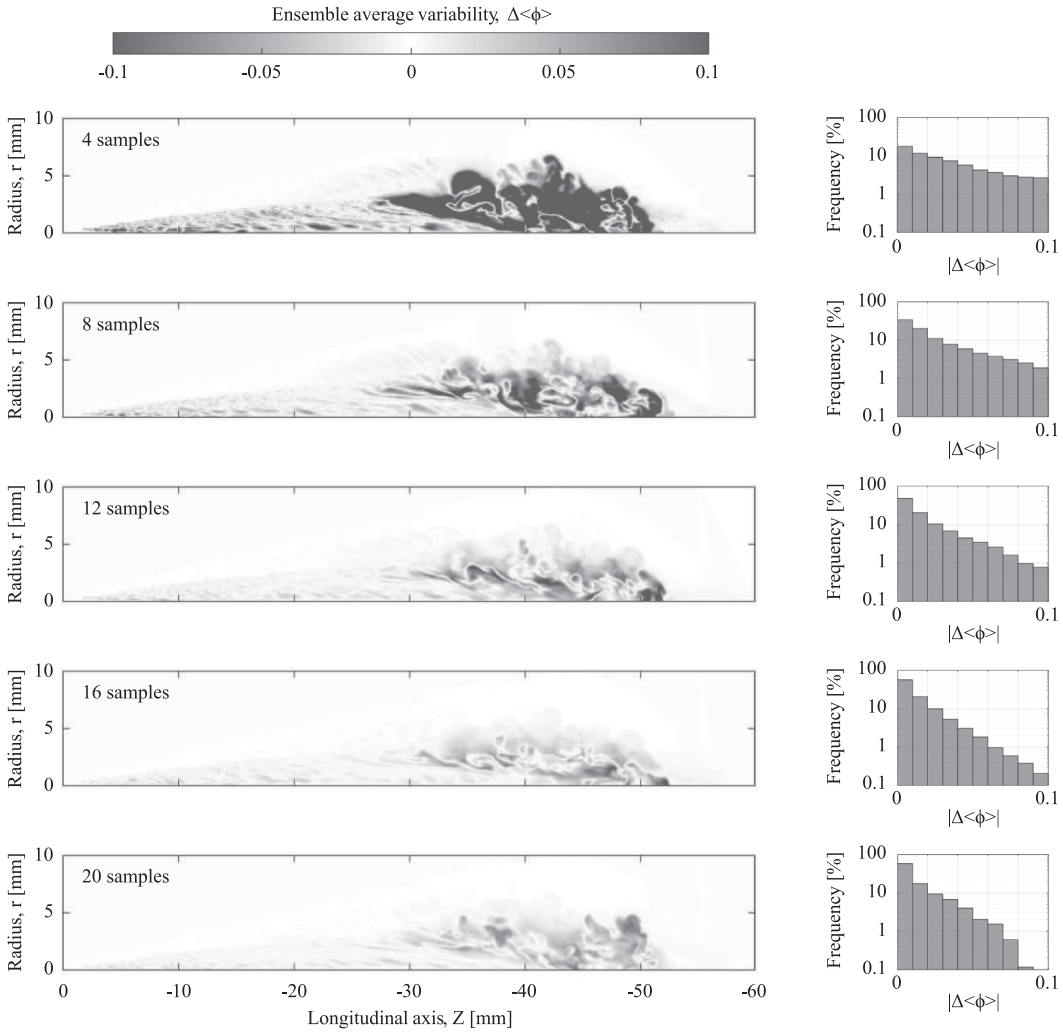

Fig. 7. Ensemble average variability for the equivalence ratio distribution on a section passing for the spray axis at 0.3 ms aSOI as a function of the considered number of samples. Associated frequency distributions on the right.

these thresholds represent the average and maximum error, due to the limited size of the statistical sample, that can be expected on the ensemble average if 20 realizations are considered. According to this computation, an average error of 1.5 m/s and a maximum error of 14 m/s is present for the |V| ensemble average, while the ϕ ensemble average features an average error of 0.02 and a maximum error of 0.11. These errors were considered sufficiently low, especially considering the typical values of |V| and ϕ reached by a diesel spray (e.g., see Fig. 3 for this case study). Furthermore, the maximum error is reached only in very few locations of the domain, as can be seen in Fig. 7 from both the spray picture and the histogram associated with the 20 samples average. Therefore, the defined accuracy limits were considered in line with the scope of the work.

3. Results and discussion

3.1. Free spray

As reported in Table 4, the multi-slice ensemble average approach, as set in this work, involves running just 25% of the original number of simulations, if a 2D representation of the results is sufficient. However, in dealing with LES spray simulations, the statistics of several macroscopic parameters (e.g., spray tip penetration or Sauter Mean Diameter (SMD)), which are intrinsically related to the 3D distribution of the liquid parcels, can be affected by the lower number of samples, in this case passing from 20 of the standard approach to 5 of the multi-slice approach. Therefore, it is important to verify that this lower number of samples can be acceptable for these parameters, from a statistical convergence point of view.

In Fig. 9, the ensemble-averaged liquid and vapor penetrations as a function of time are illustrated for both 20 samples and 5 samples statistics, together with the associated standard deviation (σ). The simulated liquid penetration is herein defined as the radius of a sphere centred in the nozzle hole which contains 95% of the total liquid mass at each time instant, while the vapor penetration is the largest distance between the nozzle hole and the cells which feature a fuel vapor mass fraction higher than 0.1%. Moreover, experimental liquid penetration is depicted with empty circles to easily evaluate the accuracy level of the calibrated spray model [15].

Focusing on the penetration curves (Fig. 9 – bottom), it can be observed that the LES ensemble averages (solid lines) are almost identical considering 20 samples (black) or 5 samples (red). This is confirmed also for the standard deviation bands, which are almost overlapped, highlighiting a similar variability, despite the different sample size. It is worth to note the high predictive capability of the 3D-CFD spray model in terms of liquid penetration, if compared with the experimental data (grey circles).

The influence of the number of samples on the average drop sizing

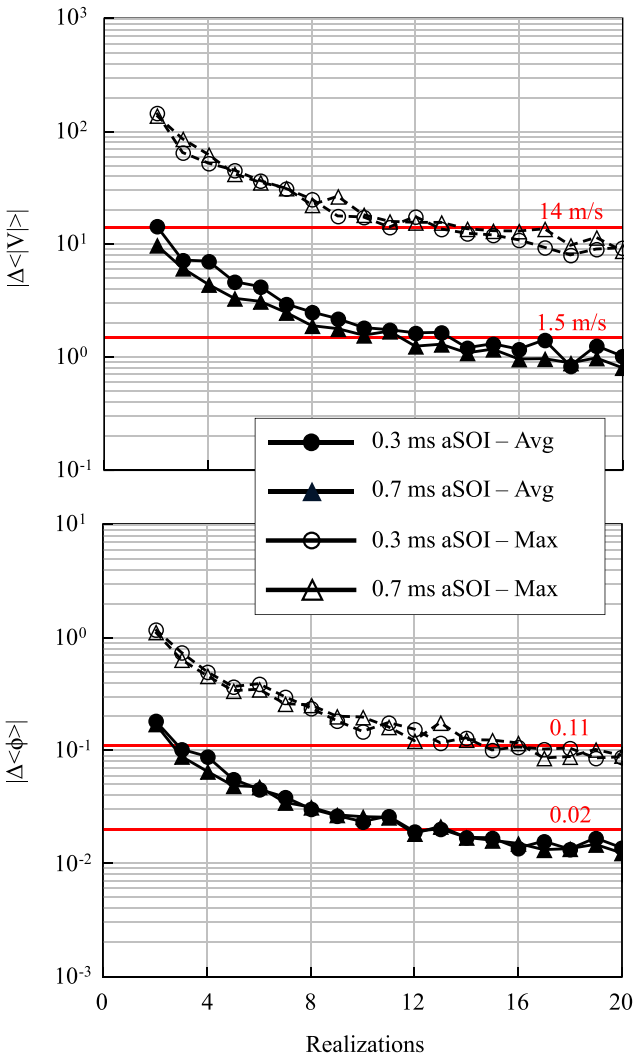

Fig. 8. Average (solid line) and maximum (dashed line) values of the variability distributions (Fig. 7) as a function of the considered number of realizations for both velocity magnitude (top) and equivalence ratio (bottom). A transient (0.3 ms aSOI – circle) and a pseudo-stationary (0.7 ms aSOI – triangle) time instants are considered. Stability thresholds are highlighted in red. (For interpretation of the references to color in this figure legend, the reader is referred to the web version of this article.)

was also evaluated, measuring the SMD value across a certain temporal window in several evenly spaced locations, placed on a segment orthogonal to the spray axis (named *Y Traverse*) at 50 mm axial distance from the nozzle, as experimentally executed in [15] for a different operating condition. In Fig. 10, these average SMD values are illustrated for both 20 samples and 5 samples statistics. As above, the variability among the different cases is also reported in terms of standard deviation bands.

The SMD average values (solid lines) are almost overlapped between 20 samples (black) and 5 samples (red) statistics for most of the spatial window, with a slight deviation when the spray periphery is approached for negative Y traverse values. Concerning the standard deviation bands, when only 5 samples are considered, the dispersion on the average values seems slightly underestimated or overestimated by looking at positive or negative Y traverse values, respectively.

In general, from both Fig. 9 and Fig. 10, it emerged that in the LES framework the average spray macroscopic characteristics are only slightly affected by the number of samples considered for the average, due to a relatively low event-to-event dispersion. Therefore, the employment of the multi-slice ensemble average approach, targeted at a 2D representation of the simulation results at a lower computational cost, does not affect the quality of the average spray global parameters, despite the lower number of statistical samples. These results are in line with the LES results in [27], in which Senecal et al. concluded that even a single injection event can be run when looking at spray global parameters since the predictions among different injections are very similar.

Given this basis, the standard approach and the multi-slice approach outcomes can be compared in terms of spray structure on the average longitudinal semi-slice. In Fig. 11, the ensemble-averaged velocity magnitude and ϕ fields at various time instants are depicted for both the standard and the multi-slice approaches. The injector nozzle is located at r = 0 mm, Z = 0 mm.

From an overall point of view, the ensemble averages approaches provide very similar results in terms of both velocity magnitude (Fig. 11 – left) and equivalence ratio (Fig. 11 – right) field. In particular, the outcome is almost identical until the spray breakup process begins, at about 30 mm axial distance. When the spray reaches the highly turbulent region, some local differences emerge, despite not being significant from a macroscopic perspective. To systematically quantify the impact of these local differences on the full picture, two similarity indices are introduced: the Structure Similarity Index (SSI) and the Magnitude Similarity Index (MSI), reported in equations (9) and (10), respectively.

$$SSI = \frac{(m_i, n)}{\|m_i\| \bullet \|n\|} \tag{9}$$

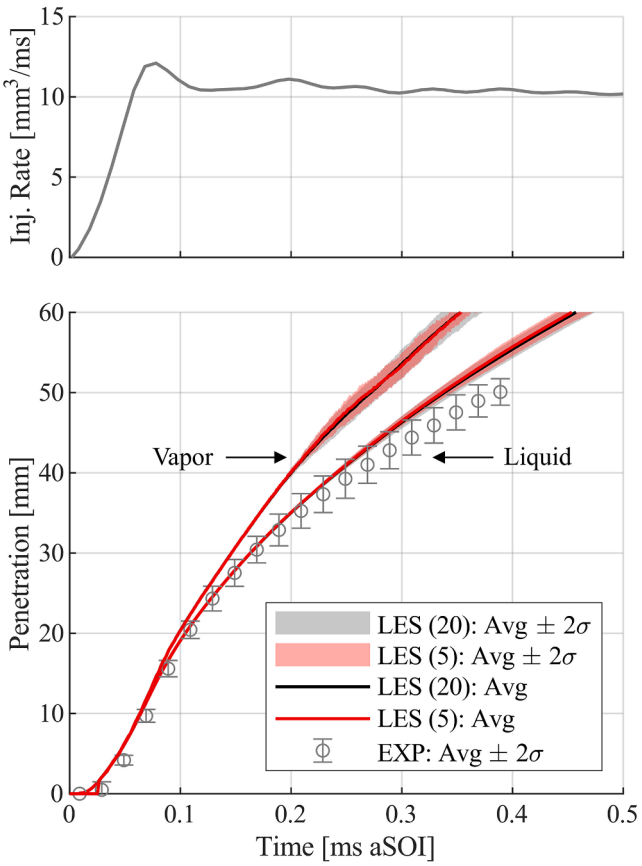

Fig. 9. Spray liquid and vapor penetrations (bottom) as a function of time for the LES, both 20 samples (black) and 5 samples (red) statistics, and the experiment (grey circles). The average (solid lines) and the standard deviation (shaded bands) are both represented. The injection rate is reported on the top. (For interpretation of the references to color in this figure legend, the reader is referred to the web version of this article.)

$$MSI = 1 - \frac{\|m_i - n\|}{\|m_i\| + \|n\|} \tag{10}$$

According to their definition [33], m_i and n represent vectors collecting the data related to two different pictures that must be compared: m_i is the picture under test, and n is the target picture. In this case, n is the ensemble average computed with standard approach on all the 20 available samples (equation (12)), while m_i is the ensemble average computed with standard or multi-slice approach considering only a certain number of samples (i) lower than 20 (equation (11)):

$$m_i = < |V|, \phi >_{Std/MS} (i \ samples) \tag{11}$$

$$n = < |V|, \phi >_{std} (20 \ samples) \tag{12}$$

Therefore, the behaviour of m can be studied as i increases, and thus the similarity with n, comparing the standard and the multi-slice approach. It is important to underline that, when i is equal to 20, m and n represent by definition the same vector, if m is computed with the standard approach. The parenthesis, (), denotes the inner product of the two vectors, and the symbol || || denotes the magnitude of the vector. If the similarity indices reach values close to 1, it means that the ensemble averages m and n are close to being identical in terms of direction (i.e., for the SSI) and magnitude (i.e., for the MSI). On the contrary, a value approaching zero means that the two flow fields are extremely different from each other.

Differently from previous studies [34], these similarity indices are not herein employed to justify the chosen number of samples as statistically sufficient, since the target vector would not be known *a priori*. In fact, given a certain number of realizations, as said above, these indices tend to reach a final value equal to 1 by definition if the standard approach is considered, without providing information on the nature of the curve if a larger number of samples would be employed in the averaging process (thus, changing the target vector). In this case, the number of samples to reach statistical convergence has been chosen with a different criterion, together with the definition of its accuracy limits (Fig. 8). Once defined that 20 samples are statistically representative of the present case study, the similarity index method is, instead, exploited to assess the validity of the multi-slice ensemble average approach with respect to the standard one, thus the target vector is well-established and fixed. In Fig. 12, the SSI and the MSI as a function of the number of considered realizations for the average are reported for both the |V| and

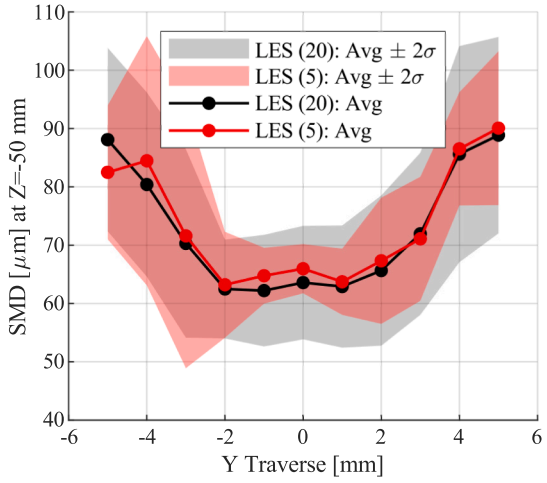

Fig. 10. SMD values, for both 20 samples (black) and 5 samples (red) statistics, at 50 mm axial distance from the injector nozzle in different locations placed on a segment orthogonal to the spray axis (i.e., Y Traverse). The average (solid line, filled circle) and the standard deviation (shaded bands) are both reported. (For interpretation of the references to color in this figure legend, the reader is referred to the web version of this article.)

ϕ fields, comparing the computation with standard and multi-slice approaches. The results are referred to a time instant (0.7 ms aSOI) in which pseudo-stationary conditions are reached within the window under analysis.

From an overall point of view, the results show very high values of similarity indices, above 0.93 even considering just two samples for the ensemble average. This manifests that, comparing the entire window with respect to the target picture, the differences are not remarkable due to the limited run-to-run variability in this case study. This is in line with the observation in Fig. 11. Therefore, the typical criterion based on fixed-value (0.9–0.95) thresholds to establish a good similarity between target and under-test pictures cannot be employed in this study. Subsequently, the graphs in Fig. 12 should be analysed from a comparative point of view, understanding the real speed-up ensured by the multi-slice approach compared to the standard approach, if an equal variability with respect to the target picture must be guaranteed.

The SSI curves (circles) are almost overlapped after 5 realizations for both the |V| field (Fig. 12 – top) and the ϕ field (Fig. 12 – bottom), achieving a value close to 1. Therefore, highly parallel vectors originate from the data collected with both ensemble average processes. For a fair comparison of the MSI curves (triangles), the last steps in which the standard curve (black) suddenly changes its slope moving towards 1 should be neglected. In fact, as above said, this value is reached by definition, thus the difference in that region cannot be used as an eligibility criterion. Hence, the MSI value achieved by the multi-slice approach (red) at 16 realizations is considered for the analysis (namely, immediately before that the slope artificially increases for the standard curve): an MSI equal to about 0.98 is achieved by the multi-slice approach for both fields. The same similarity to the target is achieved by the standard approach after 7–9 realizations. In other words, since 16 realizations are obtained using only 4 simulations with the multi-slice approach applied as in this work (i.e., 4 slices per simulation), a 50% effective reduction of the computational cost is ensured, if an equal variability with respect to the target picture is an eligibility criterion. Therefore, according to this point of view and these results, the effective speed-up (i.e., x2) operated by the multi-slice approach is lower than the theoretical one (i.e., x4). It is noteworthy that this speed-up remains still very significant, especially considering the large computational cost associated with a well-resolved LES employing statistical analyses (i.e., approximately 1520 core days for the present case study simulating the described 3D-CFD setup on the available computational resources, according to Table 4).

Dealing with the ensemble average of spray LES, the computation of the resolved Turbulent Kinetic Energy (TKE) distribution, which is correlated with high-mixing regions of the spray, is a major aspect. Therefore, the assessment of the multi-slice approach in terms of resolved TKE computation is of paramount importance before its application for high-fidelity CFD investigations. The resolved TKE was thus computed as in equation (4) for both ensemble average approaches. In Fig. 13, the resolved TKE field at various time instants is depicted for both the standard and the multi-slice approaches.

According to this computation, the resolved TKE mainly raises in the spray tip and along the spray axis, with high-TKE regions increasing in size as the spray progresses. This behaviour is captured by the multi-slice approach, confirming that the macroscopic characteristics are almost identical by adopting both ensemble average approaches. At each time instant, the high-TKE regions are similar in terms of shape and values, with only slight local variations mainly after the spray begins the breakup process. These are especially visible in the middle of the transient phase (0.3 ms aSOI), when the multi-slice approach predicts a less turbulent leading edge of the spray and slightly lower TKE values on the back part of the spray tip, however without losing the main outcomes. These slight differences are strongly attenuated moving to the other time instants, especially when pseudo-stationary conditions are achieved in the window of interest.

To analyse these results from a more local perspective and to

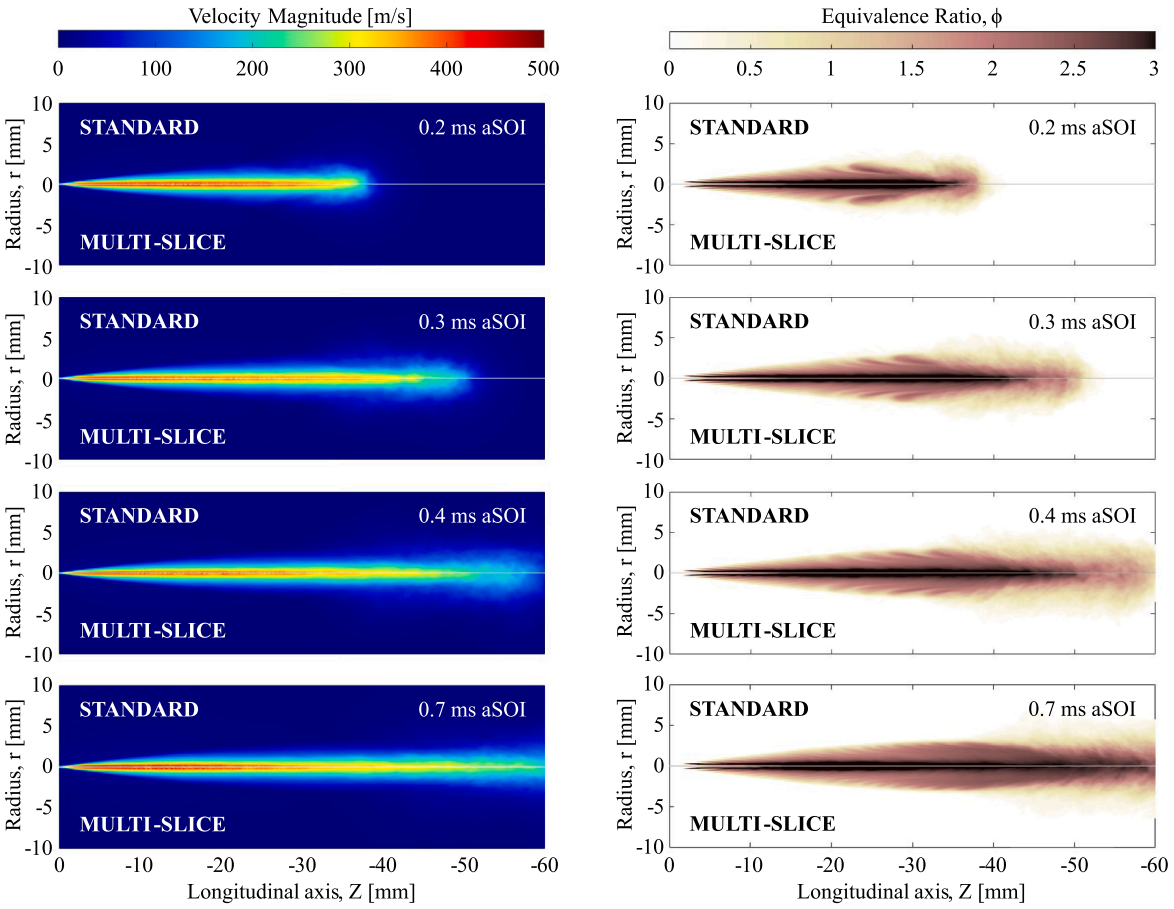

Fig. 11. Ensemble averaged velocity magnitude (left) and equivalence ratio (right) distributions on a section passing for the spray axis at several time instants: 0.2 ms aSOI, 0.3 ms aSOI, 0.4 ms aSOI, 0.7 ms aSOI. Comparison between Standard (top side) and Multi-Slice (bottom side) ensemble average approaches.

understand the most affected turbulent length scales by averaging with the multi-slice approach, the resolved TKE spectrum was computed at Z = –23 mm, r = 1 mm. This location is of interest for two main reasons. On one hand, it is a critical point for the turbulent enhancement in the DFI context (with the selected duct geometry), as will be discussed in the next section, thus guaranteeing an easier comparison of the results. On the other hand, it is close to the expected Lift-Off Length (LOL) region for the free spray configuration, according to the combustion simulations in [19], when the same injector (i.e., the same spray model) was adopted. Thereby, in Fig. 14, the resolved TKE as a function of the turbulent frequency (i.e., TKE spectrum) is reported in logarithmic scale for both the standard approach and the multi-slice approach at the selected location.

First of all, it is important to note that both curves highlight an extended resolution of the inertial sub-range, identified by the linear part of the spectrum with an angular coefficient equal to −5/3. In fact, a value equal to $1.6 \cdot 10^7$ Hz is obtained by estimating the turbulent frequency associated with the Kolmogorov length scale, as in [10], using the same values adopted for equation (2). This value is relatively close to the end of the −5/3 slope (grey dashed line), which is kept by the TKE spectrum up to more than 10^6 Hz. Hence, this is an indirect demonstration of the capability of the adopted mesh (and the associated LES spatial filter) to solve the turbulent structures up to very small sizes, as previously intended and dealt with.

Comparing the ensemble average approaches from a global perspective, the multi-slice curve (red) captures well the behaviour of the standard curve (black) for both low frequencies (larger turbulent structures) and high frequencies (smaller turbulent structures). In particular, the curves are almost overlapped throughout the resolved portion of the inertial sub-range (i.e., approximately between 100 kHz and 1000 kHz), and for most of the energy-containing range (i.e., the lowest frequencies). The maximum deviation between the spectra is instead achieved in the range of 10–100 kHz, where a periodic behaviour described by two local peaks with the standard approach is not captured by the multi-slice one. In other words, this periodic behaviour is probably linked to a larger variability of the sample's initial conditions, which seems not representable by varying its angular position. However, since this deviation at intermediate frequencies is very short in terms of duration and occurs towards the end of the energy-containing range, thus having a limited impact on the final TKE outcome, it can be considered negligible for the purpose of this kind of evaluation.

In conclusion, in the context of free spray CFD simulation, the differences between the ensemble average approaches are very low in terms of both spray main physical quantities and turbulence characteristics, both globally and locally. Therefore, the herein assessed multi-slice approach, as applied in this work, can be a valid tool to strongly reduce the computational cost by 50–75% (i.e., according to the prescribed requirements) while still maintaining a high level of results accuracy, as mandatory for research investigations applying LES combined with statistics.

3.2. *Application of the method to the DFI configuration*

In order to validate the multi-slice ensemble average method also for LES investigation concerning the DFI technology, a similar analysis was carried out on the DFI case study presented in [15,16] under the same operating conditions reported in Table 1. This step was deemed

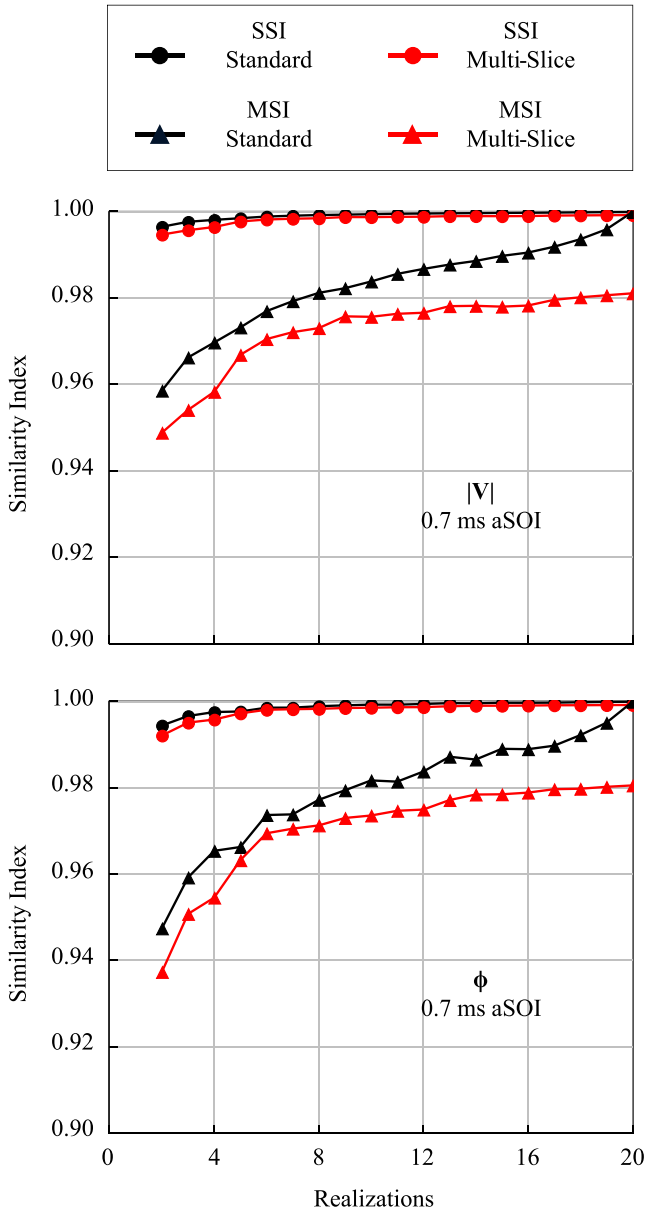

Fig. 12. Structure Similarity Index (SSI – circles) and Magnitude Similarity Index (MSI - triangles) as a function of the number of realizations for the velocity magnitude (top) and equivalence ratio (bottom) fields at 0.7 ms aSOI. Comparison between standard approach (black) and multi-slice approach (red). (For interpretation of the references to color in this figure legend, the reader is referred to the web version of this article.)

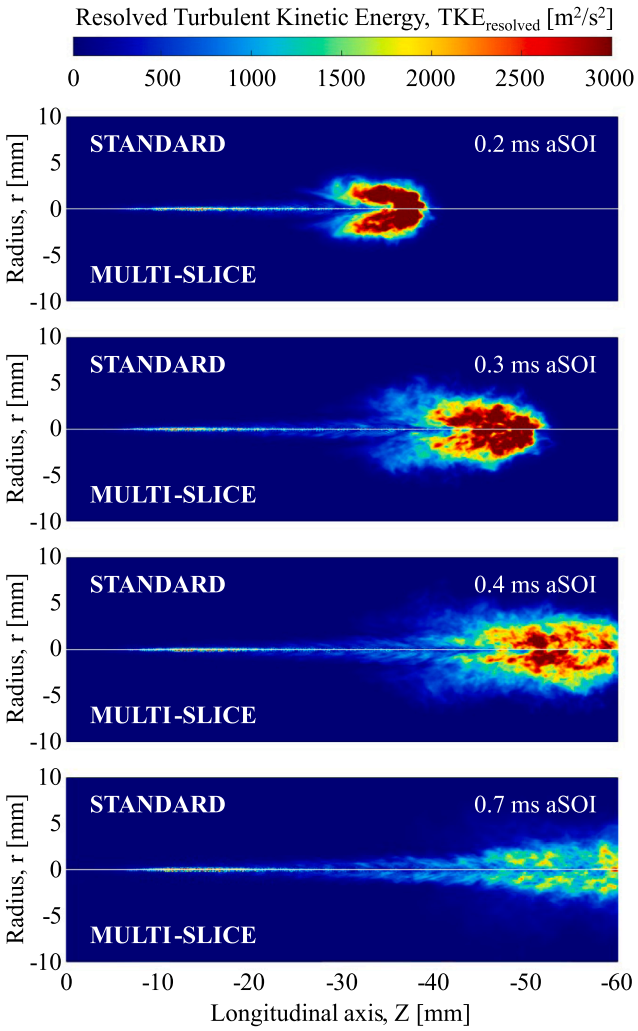

Fig. 13. Resolved Turbulent Kinetic Energy distribution on a section passing for the spray axis at several time instants: 0.2 ms aSOI, 0.3 ms aSOI, 0.4 ms aSOI, 0.7 ms aSOI. Comparison between Standard (top side) and Multi-Slice (bottom side) ensemble average approaches.

necessary to guarantee that the interaction between the spray and the duct wall does not affect the capability of the multi-slice ensemble average method to provide accurate results.

The duct geometry features a duct diameter (D) of 2 mm, a duct length (L) of 14 mm, and a stand-off distance (G) of 2 mm. The usage of the same duct geometry allows an easier comparison with the RANS results presented in [15,16]. In Fig. 15, a sketch of the DFI configuration in the CVV is reported and the main duct geometrical features are highlighted.

The 3D-CFD setup was properly modified for a correct simulation of the impact between the spray and the duct wall. In particular, a fixed refinement was adopted to reach the minimum grid size (62.5 μm) inside the whole duct volume (depicted in Fig. 15), and an inlaid mesh at the duct wall was extruded to well describe the curvature without excessive increase of cartesian cells density and to guarantee axial symmetry characteristics of the mesh (not achievable with the cartesian grid) in the spray/wall interaction region, a critical aspect for the success of the multi-slice approach. This latter feature was also of particular importance for the proper application of the Werner and Wengle wall function [35], enabling an additional degree of freedom to make the non-dimensional wall distance (y_+) fall within the suggested range along the entire inner wall of the duct. In fact, given the prohibitive computational cost associated with the resolution of the boundary layer for high-Reynolds number applications, the so-called LES Near Wall Modelling (LES-NWM) approach was adopted, based on the law of the walls [36]. The grid settings were accurately evaluated with the same criteria proposed in section 2.2 for the free spray case, leading to a high-quality LES resolution in most of the domain, in line with the purpose of this study. Finally, the rebound/slide model was employed for spray/wall interaction [37,38], because it outperformed the other available wall film model in this case study, despite its conceptual simplicity. In particular, in the RANS framework [15], it allowed good predictive capability without any modification of the spray model, calibrated on the free spray experimental data.

This multi-slice approach assessment for the DFI configuration was set as in the free spray case (Table 4), comparing its ensemble average on 20 samples (i.e., 5 differently initialized simulations) with respect to the

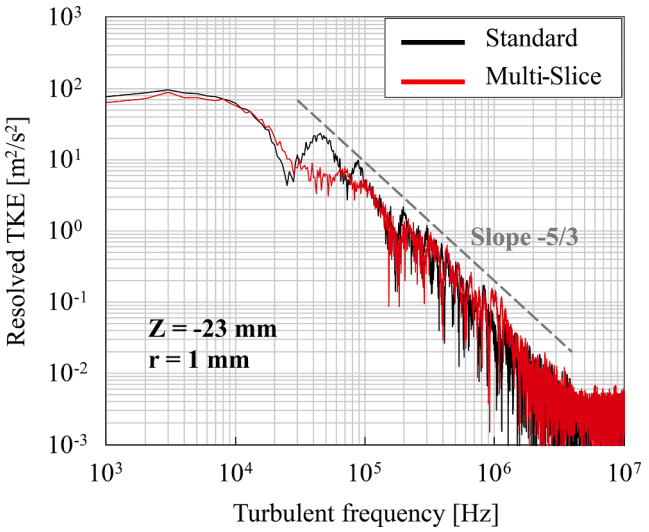

Fig. 14. Resolved Turbulent Kinetic Energy spectrum at a selected location (Z = –23 mm; r = 1 mm), computed with both Standard (black) and Multi-Slice (red) ensemble average approaches. (For interpretation of the references to color in this figure legend, the reader is referred to the web version of this article.)

ensemble average on 20 samples obtained with the standard approach (i.e., 20 differently initialized simulations). Obviously, compared to the free spray case, a variation of the total runtime was observed, in line with the different number of cells and the minimum time-step reached in the DFI simulations.

In Fig. 16, the ensemble-averaged velocity magnitude field is depicted for both the standard and the multi-slice approaches at 0.7 ms aSOI, namely in pseudo-stationary conditions considering the spatial window of interest.

It can be observed that the multi-slice picture (bottom) is almost identical to the standard one (top), correctly describing the behaviour of the duct inflow and outflow, the velocity increment inside the duct, and the gradual velocity reduction after the duct exit due to the momentum transfer from the spray to the surrounding air. The radial enlargement of

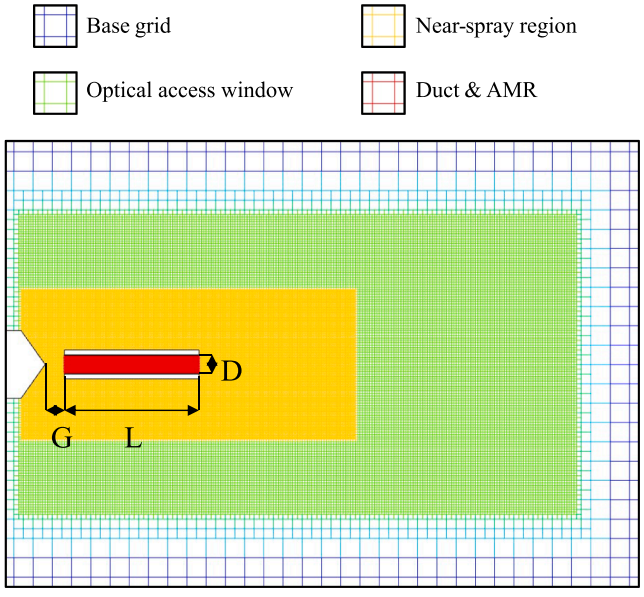

Fig. 15. DFI configuration: main duct geometrical features, grid discretization, and refinements. The base grid and the fixed refinement regions are illustrated before the injection (inactive AMR). Minimum grid size: 62.5 μm.

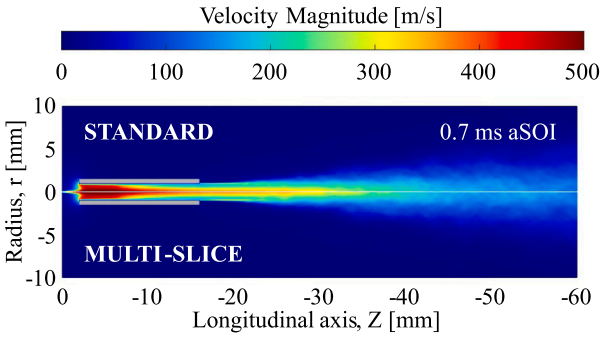

Fig. 16. Ensemble averaged velocity magnitude distribution on a section passing for the spray axis at 0.7 ms aSOI. Comparison between Standard (top side) and Multi-Slice (bottom side) ensemble average approaches in the DFI configuration.

the spray shape after the duct exit, highlighted by computational cells with velocity values higher than the test vessel, is almost specular between the standard approach and the multi-slice one.

As carried out for the free spray case, the SSI and the MSI indices (equations (9) and (10)) were employed to understand the impact of the local differences on the full ensemble average picture. In Fig. 17, the SSI and the MSI as a function of the number of considered realizations for the average are reported for both the |V| and ϕ fields at 0.7 ms aSOI, comparing the computation with standard and multi-slice approaches.

As in the free spray case, the SSI curves (circles) are very close to 1 after a few realizations for both the |V| (Fig. 17 – top) and the ϕ (Fig. 17 – bottom) fields, and almost overlapped between standard (black) and multi-slice (blue) approaches. Therefore, the associated vectors are highly parallel also with the DFI configuration. Focusing on the MSI results (triangles), it is evident how the final slope of the standard curve has a much higher final slope (i.e., immediately before reaching a value equal to 1, by definition) than the free spray case (Fig. 12). This manifests that the more intense turbulent fluctuations expected in the DFI case [15], can enlarge the variability between different samples, making the statistical convergence less forthcoming by adopting the same number of samples (i.e., 20 for the ensemble average). This makes harder the comparison between the multi-slice approach and the standard one by using these graphs since even the standard curve is less stable. The difference could be thus linked to either the application of the multi-slice approach or the not sufficiently stable average. However, considering the ensemble-averaged |V| distribution, which is less affected by the stronger turbulent fluctuations, and referring to the maximum number of realizations before the sudden slope increase of the standard curve (i.e., 12 realizations), it is still possible to examine the simulation speed-up introduced by the multi-slice approach, in the DFI case. In particular, an MSI equal to about 0.97 is achieved by the multi-slice approach after 12 realizations (i.e., 3 simulations). The same similarity to the target is achieved by the standard approach after 6 realizations (i.e., 6 simulations). In other words, the multi-slice approach, as applied in this work, guarantees a 50% effective reduction of the computational cost also in the DFI case, if equal variability with respect to the target picture is an eligibility criterion.

In Fig. 18, the resolved TKE in the selected location (Z = –23 mm; r = 1 mm) as a function of the turbulent frequency is reported in logarithmic scale for both the standard approach and the multi-slice approach. This location is of particular interest due to the triggering of the so-called second stage turbulent mixing enhancement, computed for the DFI technology with RANS simulations [15,16,19]. In fact, in that region, characterized by high-velocity gradients between spray and test vessel, the flow detachment occurs since the spray is no longer guided by the duct wall. Therefore, in this location, the accuracy of the resolved TKE computed with multi-slice ensemble average approach is of paramount importance for the DFI investigation.

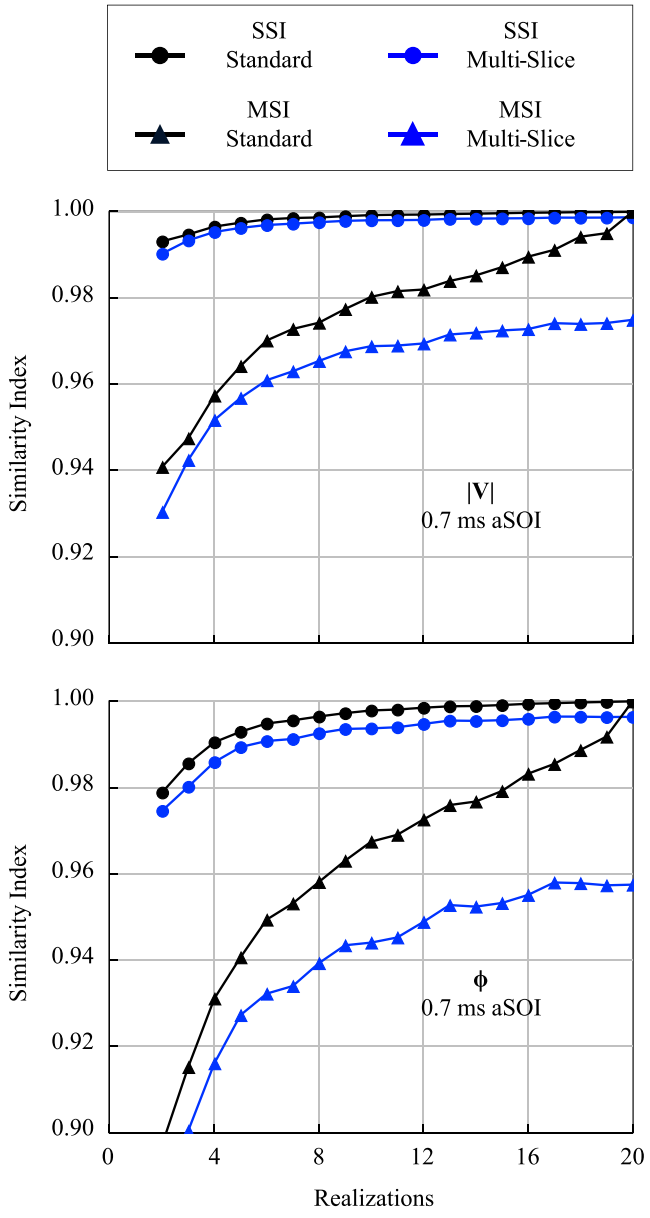

Fig. 17. Structure Similarity Index (SSI – circles) and Magnitude Similarity Index (MSI - triangles) as a function of the number of realizations for the velocity magnitude (top) and equivalence ratio (bottom) fields at 0.7 ms aSOI. Comparison between standard approach (black) and multi-slice approach (blue) in the DFI configuration. (For interpretation of the references to color in this figure legend, the reader is referred to the web version of this article.)

The resolved TKE computed with the multi-slice approach (blue) accurately reproduces the standard curve (black) throughout both the energy-containing range and resolved portion of the inertial sub-range. Compared to the TKE spectrum associated with the free spray case in the same location (Fig. 14), the multi-slice approach behaves even better in the DFI configuration, not showing any significant variation in the entire spectrum.

Finally, according to the present results, similar conclusions can be drawn for the multi-slice approach applied to a DFI case study. Indeed, the differences between the ensemble average approaches are very low in terms of both ducted spray main physical quantities and turbulence characteristics, both globally and locally, paving the way for a larger utilization of the multi-slice approach for DFI investigation through LES. Indeed, the multi-slice approach, if applied as in this work, enables a reduction of the computational cost by 50–75%, still maintaining a high level of results accuracy.

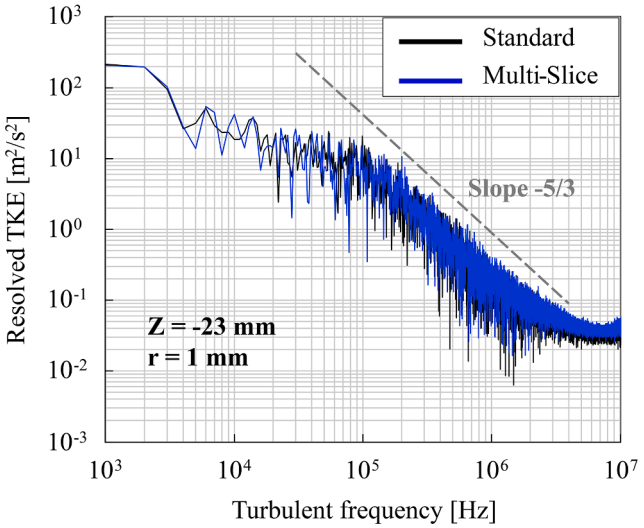

Fig. 18. Resolved Turbulent Kinetic Energy spectrum in the DFI configuration at a selected location (Z = –23 mm; r = 1 mm), computed with both Standard (black) and Multi-Slice (blue) ensemble average approaches. (For interpretation of the references to color in this figure legend, the reader is referred to the web version of this article.)

4. Conclusions

This paper proposes a methodological assessment of a runtime saving approach for the ensemble average of axial symmetric spray Large Eddy Simulations (LES). This approach was herein named *Multi-Slice* approach and was compared with the conventional (herein named *Standard*) ensemble average approach, statistical sample size being equal. A non-reacting diesel spray case study has been considered for the analysis in two different configurations: free spray and Ducted Fuel Injection (DFI). The LES 3D-CFD setup has been defined based on a thorough grid sensitivity analysis aiming at guaranteeing more than 80% of resolved turbulent structures in the whole domain of interest. A demonstration of the multi-slice ensemble average concept is provided, in terms of the accuracy of the main spray physical quantities and turbulent characteristics, as well as the discussion of the main limitations and best practices to avoid unwanted fictitious impacts on the results. In particular, the multi-slice ensemble average approach ensured accurate results for both free spray and DFI in terms of physical quantities and resolved Turbulent Kinetic Energy (TKE), both globally and locally. Moreover, the reduction of the number of samples did not affect the computation of the average macroscopic quantities (e.g., spray penetration), due to the limited event-to-event dispersion of these spray characteristics.

In conclusion, considering the multi-slice approach as applied in this study (i.e., 4 slices per simulation), a 50–75% computational cost reduction is achievable (according to the prescribed requirements), still maintaining a high level of results accuracy. This huge computational cost reduction could motivate more researchers involved in the investigation of spray processes to undertake the path of statistically significant LES analysis. Future works will exploit this method for the investigation of DFI through LES combined with statistics.

CRediT authorship contribution statement

C. Segatori: Conceptualization, Formal analysis, Methodology, Investigation, Writing – original draft. **A. Piano:** Conceptualization, Methodology, Investigation, Supervision, Writing – review & editing. **B. Peiretti Paradisi:** Conceptualization, Methodology, Investigation,

Writing – review & editing. **F. Millo:** Project administration, Supervision. **A. Bianco:** Conceptualization, Methodology.

Declaration of Competing Interest

The authors declare that they have no known competing financial interests or personal relationships that could have appeared to influence the work reported in this paper.

Data availability

The data that has been used is confidential.

Acknowledgments

Computational resources were provided by HPC@POLITO (http://www.hpc.polito.it).

Convergent Science provided CONVERGE licenses for this work.

Appendix A. Supplementary data

Supplementary data to this article can be found online at https://doi.org/10.1016/j.fuel.2023.128110.

References

[1] Stiesch G. Modelling Engine Spray and Combustion Processes: Heat and Mass Transfer. Springer; 2010. ISBN 978-3-642-05629-1.
[2] Heywood JB. Internal Combustion Engine Fundamentals. New York: McGraw-Hill; 1988. ISBN 978-1260116106.
[3] Dec JE. A Conceptual Model of DI Diesel Combustion Based on Laser-Sheet Imaging. SAE Trans 1997;1319–1348. https://doi.org/10.4271/970873.
[4] Polonowski CJ, Mueller CJ, Gehrke CR, Bazyn T, Martin GC, Lillo PM. An Experimental Investigation of Low-Soot and Soot-Free Combustion Strategies in a Heavy-Duty, Single-Cylinder, Direct-Injection, Optical Diesel Engine. SAE Int J Fuels Lubr 2012;5(1):51–77. https://doi.org/10.4271/2011-01-1812.
[5] "ECN, Engine Combustion Network: Spray A&B," https://ecn.sandia.gov/diesel-spray-combustion/target-condition/spray-ab/.
[6] Sagaut P. Large Eddy Simulation for Incompressible Flows. An Introduction. Springer; 2001. ISBN 978-3540263449.
[7] Erb A, Hosder S. Analysis and comparison of turbulence model coefficient uncertainty for canonical flow problems. Comput Fluids 2021;227:105027. https://doi.org/10.1016/j.compfluid.2021.105027.
[8] Germano M, Piomelli U, Moin P, Cabot WH. A dynamic subgrid-scale eddy viscosity model. Phys Fluids A: Fluid Dynamics 1991;3(7):1760–5. https://doi.org/10.1063/1.857955.
[9] Martínez J, Piscaglia F, Montorfano A, Onorati A, Aithal SM. Influence of spatial discretization schemes on accuracy of explicit LES: Canonical problems to engine-like geometries. Comput Fluids 2015;117:62–78. https://doi.org/10.1016/j.compfluid.2015.05.007.
[10] Pope SB, editor. Turbulent Flows. Cambridge University Press; 2000. ISBN 978-0521598866.
[11] Farrace D, Panier R, Schmitt M, Boulouchos K, Wright YM. Analysis of Averaging Methods for Large Eddy Simulations of Diesel Sprays. SAE Int J Fuels Lubr 2015;8(3):568–80. https://doi.org/10.4271/2015-24-2464.
[12] Habchi C, Bruneaux G. LES and experimental investigation of diesel sprays. ICLASS 2012 - 12th Int. Conf. Liq. At. Spray Syst.. 2012.
[13] Pitsch H, Steiner H. Large-eddy simulation of a turbulent piloted methane/air diffusion flame (Sandia flame D). Phys Fluids 2000;12(10):2541–54. https://doi.org/10.1063/1.1288493.
[14] Desantes JM, García-Oliver JM, Novella R, Pérez-Sánchez EJ. Application of a flamelet-based CFD combustion model to the LES simulation of a diesel-like reacting spray. Comput Fluids 2020;200:104419. https://doi.org/10.1016/j.compfluid.2019.104419.
[15] Millo F, Piano A, Peiretti Paradisi B, Postrioti L, Pieracci L, Bianco A, et al. Ducted Fuel Injection: Experimental and numerical investigation on fuel spray characteristics, air/fuel mixing and soot mitigation potential. Fuel 2021;289:119835. https://doi.org/10.1016/j.fuel.2020.119835.
[16] Millo F, Piano A, Peiretti Paradisi B, Segatori C, Postrioti L, Pieracci L, et al. Ducted Fuel Injection: A Numerical Soot-Targeted Duct Geometry Optimization. SAE Int J Engines 2022;15(2):297–317. https://doi.org/10.4271/03-15-02-0014.
[17] Mueller CJ, Nilsen CW, Ruth DJ, Gehmlich RK, Pickett LM, Skeen SA. Ducted fuel injection: A new approach for lowering soot emissions from direct-injection engines. Appl Energy 2017;204:206–20. https://doi.org/10.1016/j.apenergy.2017.07.001.
[18] Richards, K.J., Senecal, P.K., and Pomraning, E., "CONVERGE 3.0.14," 2022.
[19] Millo, F., Segatori, C., Piano, A., Peiretti Paradisi, B., and Bianco, A., "An engine parameters sensitivity analysis on ducted fuel injection in constant volume vessel using numerical modeling," *SAE Technical Paper* 2021-24-0015, 2021, https://doi.org/10.4271/2021-24-0015.
[20] Reitz RD, Diwakar R, Structure of high-pressure fuel sprays, *SAE Technical Paper* 870598, 1987, https://doi.org/10.4271/870598.
[21] Amsden AA, O'Rourke PJ, Butler TD, "KIVA-II: A computer program for chemically reactive flows with sprays," Los Alamos Natl. Lab. Tech. LA-11560-MS, 1989.
[22] Reitz RD, Bracco FV. Mechanisms of breakup of round liquid jets. Encycl Fluid Mech 1986;3.
[23] Liu AB, Mather D, Reitz RD, "Modeling the effects of drop drag and breakup on fuel sprays," *SAE Technical Paper* 930072, 1993, https://doi.org/10.4271/930072.
[24] Amsden AA, Findley M, "KIVA-3V: A block-structured KIVA program for engines with vertical or canted valves," Los Alamos Natl. Lab. Tech. LA-13313-MS, 1997.
[25] Chaves H, Knapp M, Kubitzek A, Obermeier F, Schneider T, "Experimental study of cavitation in the nozzle hole of diesel injectors using transparent nozzles," *SAE Technical Paper* 950290, 1995, https://doi.org/10.4271/950290.
[26] Pomraning E, Rutland CJ. Dynamic one-equation nonviscosity large-eddy simulation model. AIAA J 2002;40(4):689–701. https://doi.org/10.2514/2.1701.
[27] Senecal PK, Pomraning E, Richards KJ, Som S, "An investigation of grid convergence for spray simulations using an les turbulence model," *SAE Technical Paper* 2013-01-1083, 2013, https://doi.org/10.4271/2013-01-1083.
[28] Pomraning E. Development of Large Eddy Simulation Turbulence Models. University of Wisconsin-Madison; 2000. PhD Thesis.
[29] Senecal PK, Richards KJ, Pomraning E, Yang T et al., "A new parallel cut-cell Cartesian CFD code for rapid grid generation applied to in-cylinder Diesel engine simulations," SAE Technical Paper 2007-01-0159, 2007, https://doi.org/10.4271/2007-01-0159.
[30] Pope SB. Ten questions concerning the large-eddy simulation of turbulent flows. New J Phys 2004;6. https://doi.org/10.1088/1367-2630/6/1/035.
[31] Senecal PK, Pomraning E, Richards KJ, Som S. Grid-Convergent Spray Models for Internal Combustion Engine Computational Fluid Dynamics Simulations. J Energy Resour Technol 2014;136(1). https://doi.org/10.1115/1.4024861.
[32] Piscaglia F, Montorfano A, Onorati A. Towards the LES simulation of IC engines with parallel topologically changing meshes. SAE Int J Engines 2013;6(2):926–40. https://doi.org/10.4271/2013-01-1096.
[33] Hu B, Banerjee S, Liu K, Rajamohan D et al., "Large eddy simulation of a turbulent non-reacting spray jet," *ASME 2015 Intern. Combust. Engine Div. Fall Tech. Conf.*, 2015, https://doi.org/10.1115/ICEF2015-1033.
[34] Ameen MM, Pei Y, Som S, "Computing Statistical Averages from Large Eddy Simulation of Spray Flames," *SAE Technical Paper* 2016-01-0585, 2016, https://doi.org/10.4271/2016-01-0585.
[35] Werner H, Wengle H, "Large eddy simulation of turbulent flow over and around a cube in plane channel," 155–168, 1991.
[36] Piomelli U. Wall-layer models for large-eddy simulations. Prog Aerosp Sci 2008;44(6):437–46. https://doi.org/10.1016/j.paerosci.2008.06.001.
[37] Naber JD, Reitz RD. Modeling Engine Spray/Wall Impingement. SAE Technical Paper 1988;880107. https://doi.org/10.4271/880107.
[38] Gonzalez DMA, Borman GL, Reitz RD, "A study of Diesel cold starting using both cycle analysis and multidimensional calculations," *SAE Trans.* 189–208, 1991, https://doi.org/10.4271/910180.